

Paper-Based Multiplex Surface-Enhanced Raman Scattering Detection Using Polymerase Chain Reaction Probe Codification

Eun Ju Kim, Hanbi Kim, Eunkyong Park, Taekyung Kim, Doo Ryeon Chung, Young-Man Choi, and Minhee Kang*



Cite This: *Anal. Chem.* 2021, 93, 3677–3685



Read Online

ACCESS |



Metrics & More

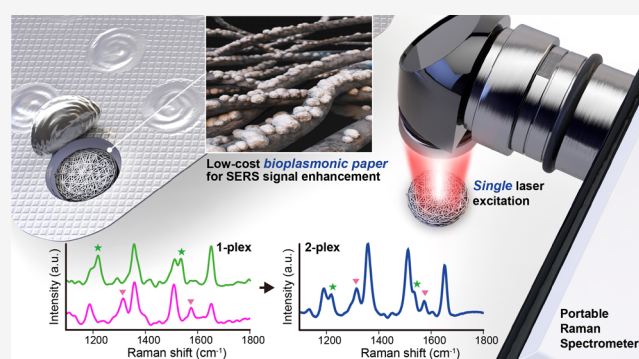


Article Recommendations



Supporting Information

ABSTRACT: We construct a multiplex surface-enhanced Raman scattering (SERS) platform based on a plasmonic paper substrate and a double-labeled probe for the detection of multiple fluorescent dyes at high sensitivity in a single-wavelength light source system. Plasmonic paper, made of silver nanodots on three-dimensional cellulose fibers, enables highly sensitive SERS biosensing based on localized surface plasmon resonance (LSPR). The proposed method enables the identification and quantification of a range of fluorescent dyes ranging from picomolar to millimolar concentrations. The use of 5' fluorescent dyes and 3' biotin-modified probes as SERS-coded probes renders possible the separation of fluorescent dyes with streptavidin-coated magnetic beads (SMBs) and the sensitive detection of multiple dyes after the reverse transcription polymerase chain reaction (RT-PCR). This experimental study reveals the multiplex detection capability of PCR-based SERS under existing PCR conditions without modifying primer and probe sequences. The combination of magnetic bead-based separation and paper SERS platform is efficient, economical, and can be used for the simultaneous detection of two or more pathogens.



Surface-enhanced Raman scattering (SERS) is a promising method for the high sensitivity detection of multiple fluorescent dyes.^{1–4} SERS offers a highly resolved vibrational fingerprint, which results from the localized surface plasmon resonance (LSPR) of noble metal nanostructures influenced by neighboring molecules, interparticle gap spacing, or geometry.^{5–9} The Raman spectra of the same fluorophores yield spectral peaks with a full-width half-maximum that is 10–100 times narrower than that observed using fluorescence emission spectra. Thus, SERS allows highly sensitive multiplex analysis and can be used in clinical and laboratory applications, including in the polymerase chain reaction (PCR), which is considered the gold standard for detecting microbial pathogens via nucleic acid amplification using fluorescent dyes. The fluorescent dyes allow the optical identification and quantification of the amplified gene product.¹⁰ SERS is capable of detecting fluorescent dyes early in the reaction with 10⁴–10⁹ times more sensitivity and specificity than conventional Raman scattering, which is an excellent analytical method used for trace detection in fields such as medical diagnosis and food safety.^{11,12}

Current SERS-PCR applications use Raman tag-modified complementary DNA sequences that hybridize within the amplicons,^{13–15} or Raman tag-labeled specific primers for amplification,^{16–18} and complementary DNA sequences against probe sequences for detection.^{19–24} It is important to

develop detection methods that do not modify the detection probes and do not expose amplification products, such as amplicons and nonhybridized probes, to the target sequence. In particular, the hands-on manipulation of amplicons during detection substantially increases amplicon carryover contamination in diagnostic laboratories, as the PCR generates approximately 10⁹ copies of the target sequence, which can lead to false positive results.^{25,26} Further, most diagnostic kits based on real-time PCR utilize Förster resonance energy transfer (FRET) quenching to monitor amplification in real-time.²⁷ Fluorophores for probe labeling include carboxy-fluorescein (FAM), 5-carboxytetramethylrhodamine (TAMRA), 6-carboxy-4',5'-dichloro-2',7'-dimethoxy-fluorescein (JOE), and indodicarbocyanine (Cy5). Fluorescence-based real-time PCR requires quantitative instrumentation, a turbidity meter, and 2 or more hours (approximately 40 cycles) for target visualization, which is not suitable for rapid diagnosis. Furthermore, it involves expensive specialized

Received: December 17, 2020

Accepted: February 17, 2021

Published: February 19, 2021



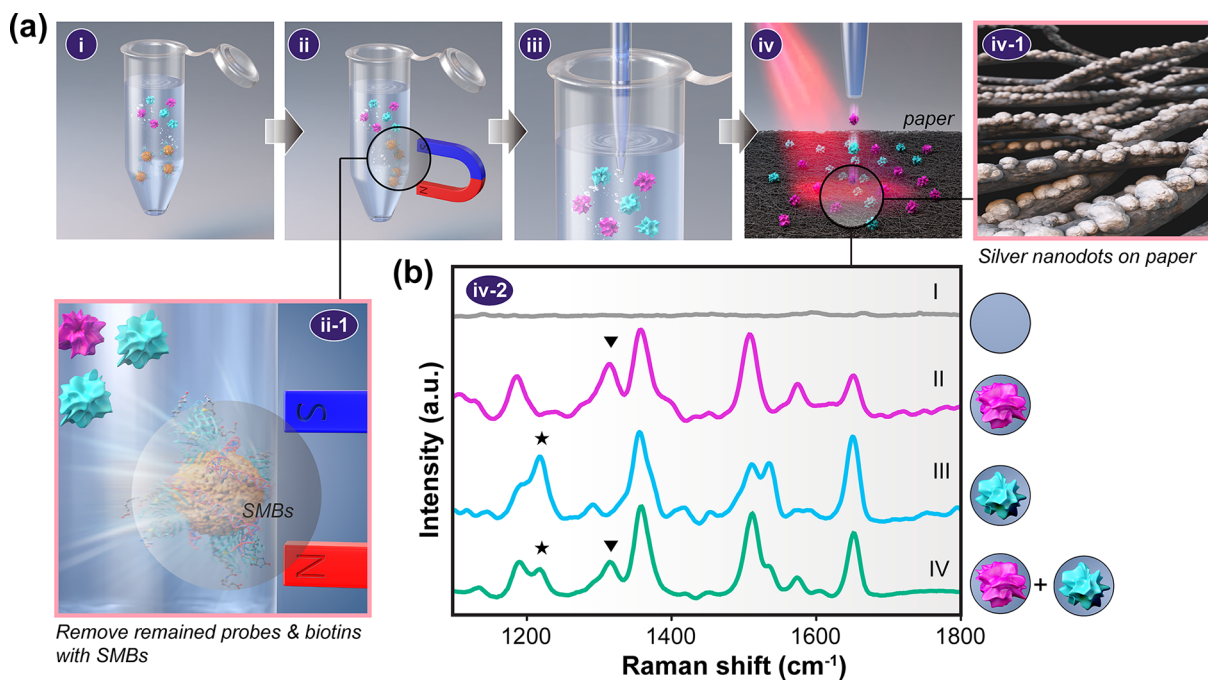


Figure 1. (a) Schematic of multiplex surface-enhanced Raman scattering (SERS) detection based on fluorophore separation and low-cost plasmonic paper. (i) Modified TaqMan probe, with a labeled fluorophore at the 5' end and biotin at the 3' end, releasing fluorescence dyes and biotin during amplification. (ii) Removal of remaining probes and hydrolytically cleaved biotin using streptavidin-coated magnetic beads (SMBs) from post-PCR product. (iii,iv) Placing the separated fluorophores as SERS-active molecules onto the silver nanodots deposited on cellulose fiber for SERS measurement. (b) Selective SERS signals of fluorophores with a single excitation wavelength. Peaks without fluorescence dye (I) and with R6G (II), TAMRA (III), and a mixture of R6G and TAMRA (IV). The characteristic peaks for R6G (1314 cm⁻¹) and TAMRA (1216 cm⁻¹) were used to indicate the presence of the target sequences.

equipment and has intrinsic limitations regarding multiplex capability (approximately 3–4) due to the broad spectrum of emissions, which often cannot be avoided due to overlapping excitation and emission wavelengths of fluorescent dyes. Therefore, the important features of the multiplex detection format are its capabilities to rapidly analyze substances (because multiple analytes must be analyzed at the same time), detect multiple targets simultaneously, and reduce test costs per assay (separate tests need not be performed).

In this study, we propose an alternative optical technique termed the multiplex PCR-based SERS platform, based on plasmonic paper substrates and a double-labeled probe, which enables the sensitive detection of numerous fluorescent dyes in a single analytical time period under existing PCR conditions without any modification of the primer and probe sequences. The plasmonic paper comprising silver nanodots on three-dimensional cellulose fibers allows highly sensitive SERS biosensing based on LSPR. The complex hierarchical ultrastructures of the cellulose fiber and quasi-ordered silver nanodots enable the identification and quantification of a range of fluorescent dyes from pico- to millimolar concentrations. Moreover, a double-labeled probe enables the separation of fluorescent dyes with streptavidin-coated magnetic beads (SMBs).^{28–30} During this process, only fluorescence dyes isolated from post-PCR products can be used for the SERS measurement as SERS-active molecules, thus minimizing carryover contamination during the detection process. The multiplex capability under existing PCR conditions without any modification of primer and probe sequences can be universally expanded to other PCR assays. To demonstrate our method, we employed the multiplex

detection capability for the detection of severe acute respiratory syndrome coronavirus 2 (SARS-CoV-2).

The multiplex PCR-SERS assay is based on fluorophore separation from the post-PCR product containing amplicons, excess primers, and probes, by using SMBs. All surplus molecules, except fluorophores as active SERS molecules, potentially contaminate and interfere with signals during SERS measurement and must be removed from post-PCR mixtures. A double-labeled probe was used as a modified TaqMan probe, with a labeled fluorophore at the 5' end and biotin at the 3' end. During PCR, the probes are hybridized onto a specific site on the target DNA, located between the forward and reverse primer positions. The nuclease activity of Taq DNA polymerase hydrolytically cleaves the probe at the 5' terminal, thereby releasing the fluorophore.^{31–33} We used SMBs to remove the remaining probes and biotin from the post-PCR product. The supernatant with the hydrolytically cleaved fluorophore was then placed on plasmonic paper for SERS measurement (Figure 1a).

PCR protocols have been designed for the detection of severe acute respiratory syndrome coronavirus 2 (SARS-CoV-2).³⁴ The virus has overwhelmed health care systems and caused social and economic disruption globally.³⁵ Several molecular targets in the positive-sense, the single-stranded RNA genome of coronaviruses, including ORF1b or ORF8, nucleocapsid (N), spike (S) protein, RNA-dependent RNA polymerase (RdRP), or envelope (E), can be used for the PCR assay.^{36–39} The World Health Organization recommends first-line screening with the E-gene assay followed by a confirmatory assay using RdRp.³⁷ The sequence information on the target gene, primers, and probes is shown in Figure S1 and Table S1. Target gene amplification with fluorophore–

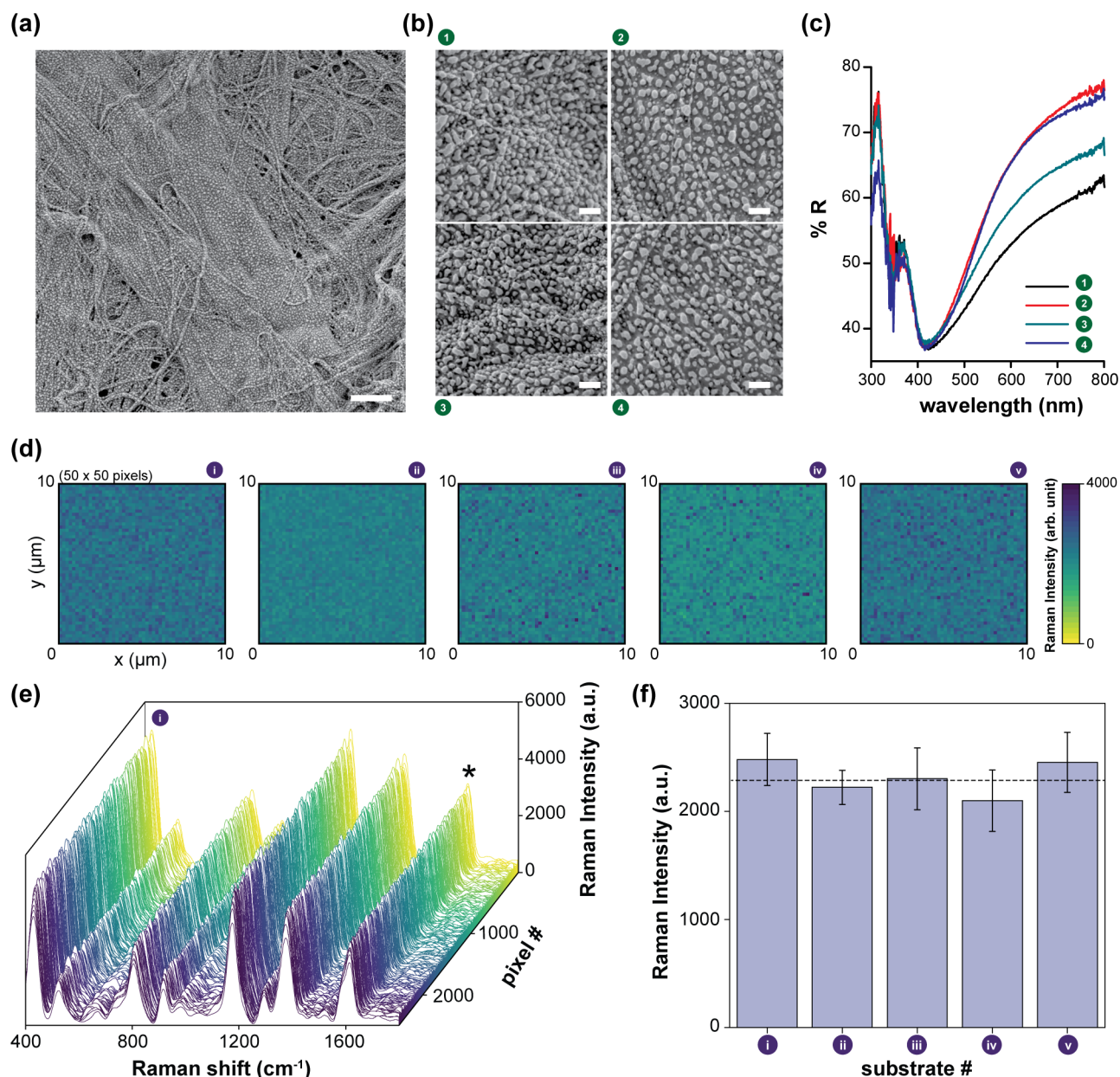


Figure 2. (a,b) Scanning electron microscope (SEM) image of silver nanodots on cellulose fiber at different times and temperatures of thermal annealing. (Annealing temperature is 170 and 180 °C for 1 h (①, ③) and 3 h (②, ④), respectively). The deposited thin silver film modified by thermal annealing forms silver nanodots, which enhances SERS signals (scale bar = 200 nm). (c) UV-vis reflectance spectra depending on silver nanodot. (d) SERS mapping images of 10^{-6} M MGITC at 1615 cm^{-1} for five different substrates (i–v) demonstrating substrate-to-substrate reproducibility. The scale bar on the right shows the color coding used to depict SERS intensity. (e) SERS spectra obtained from all the mapping points in the (i) substrate. (f) Averaged SERS intensity variations for five substrates (i–v).

biotin-coded probes and TaqMan probes was performed following conventional PCR protocols (see the experimental section in the [Supporting Information](#)). The feasibility of this assay was confirmed by conventional real-time PCR using TaqMan probes ([Figure S2](#)), and all samples were compared at 25 cycles. Rhodamine 6G (R6G) and 5-carboxytetramethylrhodamine (TAMRA), known as structural isomers of rhodamine, were labeled at the 5' end of each probe for targeting E and RdRP, respectively.

The SERS signals of the two fluorophores were measured using laser light at an excitation wavelength of 633 nm. The characteristic peaks used for identifying R6G and TAMRA are shown with asterisks. The main spectral features of TAMRA

were observed at 1216 , 1358 , 1512 , 1537 , and 1652 cm^{-1} , whereas those of R6G were observed at 1186 , 1314 , 1358 , 1512 , and 1652 cm^{-1} .⁴⁰ Representative spectra for the one- and two-plex assays are shown in [Figure 1b](#). Despite a few overlaps, the two spectra have characteristic peak profiles. We considered the characteristic peak to be 1314 cm^{-1} for R6G and 1216 cm^{-1} for TAMRA.

Bioplasmonic paper was fabricated on a large scale by low-temperature solid-state dewetting of a thin silver film on cellulose paper.^{41–43} The deposited thin silver film formed complex hierarchical silver nanodots⁴⁰ on the cellulose fiber via thermal annealing ([Figure 2a](#)). The scanning electron microscope (SEM) image illustrates the silver nanodot

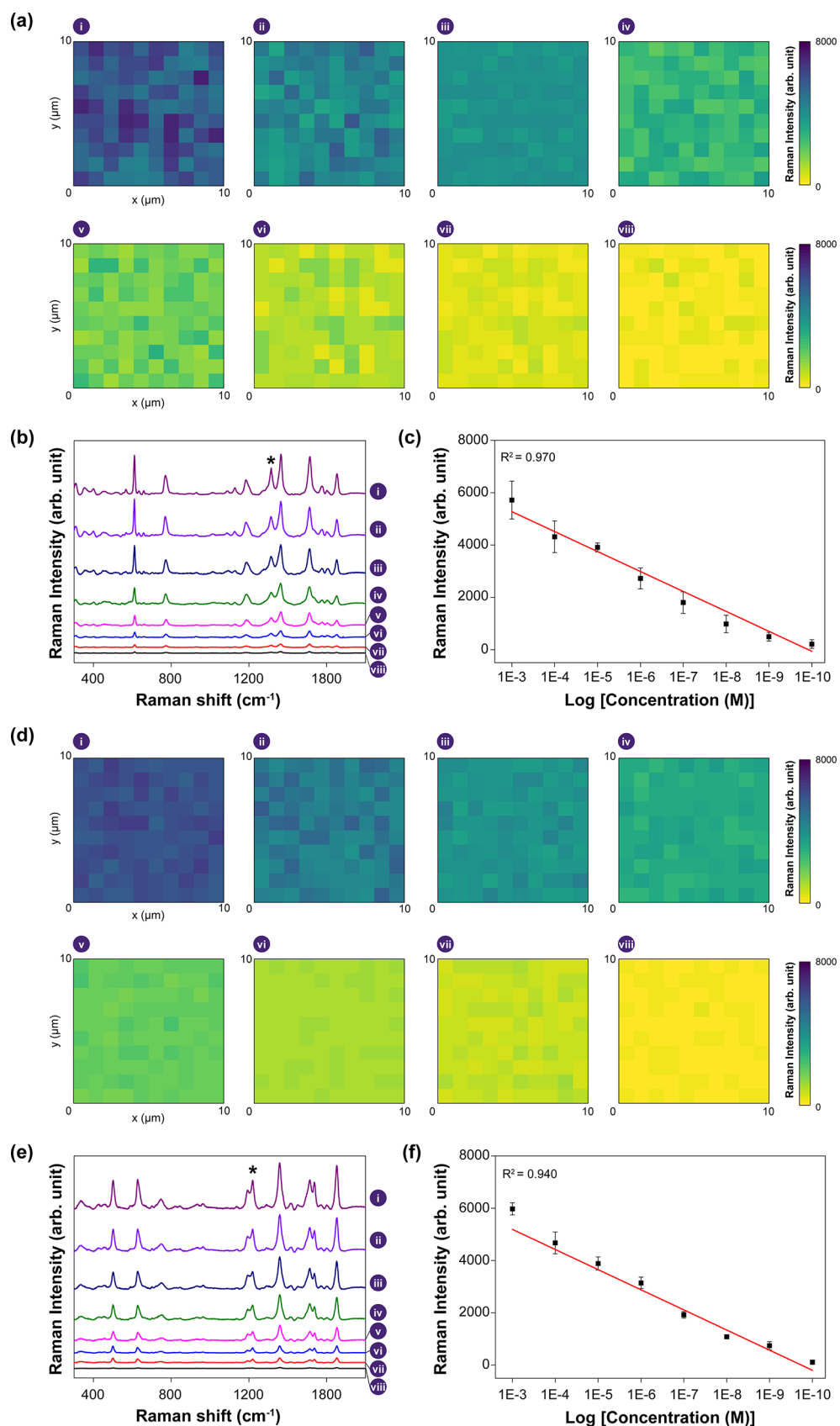


Figure 3. Concentration-dependent surface-enhanced Raman scattering (SERS) intensity. (a,d) SERS mapping images of R6G and TAMRA, measured at 1314 and 1216 cm⁻¹, respectively, ranging from 1 mM to 100 pM. The scale box on the right shows the color decoding box for SERS intensity. (b,e) Average SERS spectra from 100 points mapping data. (c,f) Calibration curves for various concentrations.

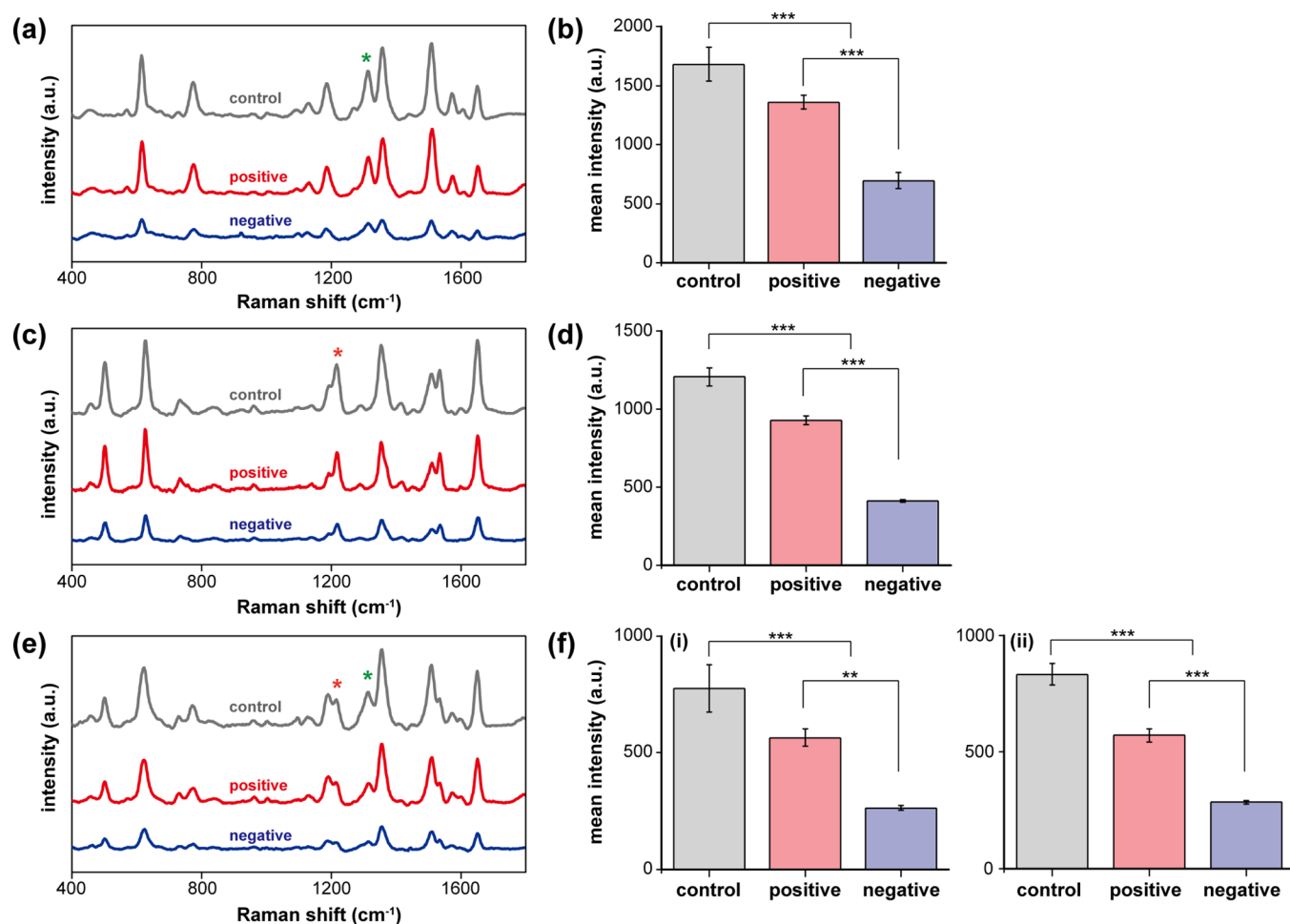


Figure 4. (a–d) Surface-enhanced Raman scattering (SERS) signal analysis of probes targeting envelope (E) and RNA-dependent RNA polymerase (RdRP) genes after separation using the postone-plex PCR assay. Rhodamine 6G (R6G) and 5-carboxytetramethylrhodamine (TAMRA) were labeled at the 5' end of each probe for targeting E and RdRP genes, respectively. Average SERS spectra and mean intensity of (a,b) R6G at 1314 cm⁻¹ and (c,d) TAMRA at 1216 cm⁻¹ of 10 different locations of bioplasmonic paper for positive (red line) and negative (blue line) samples. Post-PCR product without the separation step was prepared as a control (black line). (e,f) SERS signal analysis after the separation step using the post-two-plex PCR assay. (e) Average SERS spectra of 10 different locations of bioplasmonic paper shows a complex superposition of the independent spectra of R6G and TAMRA. The characteristic peaks of R6G and TAMRA used for identification and quantification are marked with asterisks. (f) Mean intensity at 1314 and 1216 cm⁻¹ for control, positive, and negative samples (**: *p*-value < 0.01, ***: *p*-value < 0.001).

deposits on the fibers at different times and temperatures of thermal annealing in Figure 2B; however, plasmon resonance is observed at approximately 420 nm, despite the altered annealing conditions (Figure 2c). Highly dense and uniform EM hotspots are crucial for achieving enhanced SERS signals. In this experiment, we used thermal annealing bioplasmonic paper with maximum surface coverage and EM hotspots (annealing at 170 °C for 1 h). Subsequently, SERS spectra of five different substrates were obtained by mapping the selected sample area (10 × 10 μm²) using ×10⁻⁶ M malachite green isothiocyanate (MGITC). The SERS signal intensities at 1615 cm⁻¹ were mapped, and no obvious variations were observed across the selected area (Figure 2d,e). The relative standard deviation (RSD) of the SERS signal intensities is 12.56%, which is lower than that of commercial SERS substrates⁴⁴ (Figure 2f).

To determine the substrate detection limit, R6G and TAMRA were prepared by diluting the stock solution from 1 mM to 100 pM. Concentration-dependent SERS spectra were obtained by mapping the selected sample area (10 × 10 μm²) to minimize error deviation by spot-to-spot fluctuation of the

peak intensity (Figure 3a,d). The SERS spectra obtained from all the mapping points and averaged SERS spectra with respect to concentration are shown in Figure S3 and Figure 3b,e. The averaged SERS intensities for the characteristic peaks of R6G and TAMRA at 1314 and 1216 cm⁻¹ depending on concentration showed a linear correlation, ranging from 0.1 nM to 1 mM. To achieve reliable quantification for analyzing target molecules in the sample, the coefficient of determination (*R*²) was confirmed to be greater than 0.9 for both correlations (Figure 3c,f). Under the highly predictable value, the limit of detection (LoD) was found to be 153.53 and 230.37 pM for R6G and TAMRA, respectively, which were defined by the IUPAC standard equation.⁴⁵

After PCR amplification, the fluorophores were separated from the hydrolyzed probes using the streptavidin–biotin interaction. Manual magnetic bead separation was performed for 20 s using 500 μL of SMBs with 250 μL of post-PCR mixtures that were incubated at 25 °C for 3 min. The post-PCR product without magnetic separation was prepared as a control. For fluorescence measurement, two different filter sets for green (λ_{ex} = 520 ± 10 nm, λ_{em} = 558 ± 12 nm) and yellow

($\lambda_{\text{ex}} = 549.5 \pm 10$ nm, $\lambda_{\text{em}} = 586.5 \pm 10$ nm) are used, as these two isomeric probes have different excitation and emission wavelengths, including $\lambda_{\text{ex}} = 526$ nm, $\lambda_{\text{em}} = 555$ nm for R6G and $\lambda_{\text{ex}} = 557$ nm, $\lambda_{\text{em}} = 583$ nm for TAMRA. Thus, R6G and TAMRA cannot support multiplexing in three-channel real-time PCR instead of five- or six-channel real-time PCR. However, SERS can be multiplexed with a single wavelength, and the system can be used at a relatively low cost.

Prior to demonstrating the feasibility of this multiplex PCR-SERS assay, a one-plex PCR assay was performed. Samples before and after the separation step were placed on the bioplasmonic paper for SERS analysis. The average SERS spectra of 10 different locations of bioplasmonic paper are shown in Figure 4a for positive and negative samples after separation. The post-PCR product without the separation step was used as a control. In the presence of the target sequence, that is, a positive sample, the hydrolyzed fluorophore (SERS-active dye) released during PCR and Raman signals of the fluorophores in the supernatant was revealed by SERS analysis. In contrast, in the absence of the target sequence (i.e., negative sample), the probe remains intact and is subsequently attached to the SMBs. In this case, no Raman signal was present in the sample solution. Each probe for targeting E and RdRP after the separation step indicates the SERS spectra of R6G and TAMRA, respectively, in the presence of the target sequence. The relatively weak SERS signal in the negative sample appears from unbound probes during the separation step. The characteristic peaks of R6G and TAMRA that are commonly used for identification and quantification are marked with asterisks (1314 and 1216 cm^{-1} , respectively). When calculating the characteristic peak intensity obtained at 10 different spectra, a relatively consistent signal intensity and a reliable difference between the positive and negative results for each target were observed. These results indicate the effective identification of the target sequence.

Subsequently, two-plex PCR was performed using two probes targeting R6G and TAMRA of E and RdRP genes, respectively (Figure 4b). Notably, identifying effective SERS signals from multiple fluorophores with multiplex assay is likely to be significantly different depending on numerous factors, including differences in surface adsorption characteristics, absorption maxima at the laser excitation wavelength, relative SERS cross-section, and the background fluorescence of each molecule.⁴⁶ Thus, to obtain similar intensities of SERS signals from each fluorophore, the concentration ratio of the two probes was determined by SERS analysis, because the fluorescence background of TAMRA in SERS signals made distinguishing R6G in the multiplex assay with TAMRA challenging. Similar peak intensities were identified when the concentration ratio of R6G to TAMRA was 1.4 (Figure S4). Thus, a two-plex PCR assay was performed by fixing the concentration ratio to 1.4. After separation, the samples were placed on bioplasmonic paper for SERS measurement. The average SERS spectra shown in Figure 4c revealed the complex superposition of independent spectra of R6G and TAMRA when both target sequences are present. The calculation of the intensities of the two characteristic peaks obtained at ten different spectra yielded statistically significant results (***: $p < 0.001$).

The selectivity of the PCR-SERS assay was also measured using post-PCR mixtures with two probes, by fixing the concentration ratio of R6G to TAMRA to 1.4 and employing one target gene. The SERS spectra before the separation step

showed a superposition of the R6G and TAMRA spectra, whereas characteristic peaks in the presence of the gene gradually emerged as those for the absence of the gene disappeared (Figure 5a,c). The relative peak intensity ratio

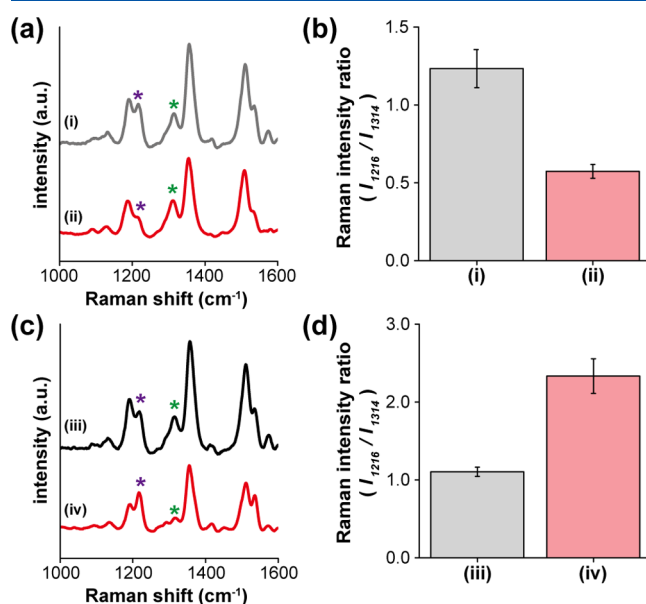


Figure 5. Selectivity of PCR-surface-enhanced Raman scattering (SERS) assay before and after separation. (a) (i) post-PCR mixture with two probes (E and RdRP) and one target gene (E); (ii) after separation for (i). (c) (iii) post-PCR mixture with two probes (E and RdRP) and one target gene (RdRP); (iv) after separation for (iii). Relative peak intensity ratio (I_{1216}/I_{1314}) before and after separation step.

(I_{1216}/I_{1314}) after the separation step is shown in Figure 5b,d. For the post-PCR mixture sample as a control, the ratio was close to one; for samples after separation, a decrease in the ratio in the presence of the E gene and an increase in the ratio in the presence of the RdRP gene was observed. These results show that our multiplex PCR-SERS assay has an advantage over fluorescence detection in terms of selectivity and ability to recognize multiple targets in the single-wavelength light source investigation.

The assay detection limits of real-time PCR and SERS-PCR were compared with 0.01 and 0.001 $\text{ng}/\mu\text{L}$ template concentrations for the E and RdRP genes. The relationships between the fluorescence intensity of the two-plex real-time PCR assay and the cycle number are plotted in Figure 6a,b. The insets show amplification plots of the real-time PCR assay for the 0.001 (blue line) and 0.01 $\text{ng}/\mu\text{L}$ (red line) concentrations. The SERS intensity of the two-plex SERS-PCR assay is plotted in Figure 6c,d. The logistic fittings of the SERS intensity depending on the cycle number for 0.01 (blue line) and 0.01 $\text{ng}/\mu\text{L}$ (red line) are shown with $R^2 > 0.99$. Note that it was impossible to detect template concentrations under 1 $\text{pg}/\mu\text{L}$ (13.64 pM for the E gene and 13.4 pM for the RdRP gene) using real-time PCR before the number of cycles reached 20. However, SERS-PCR enabled DNA detection after only 10 cycles. The relative standard deviation (RSD) of the SERS signal intensities of 10 $\text{pg}/\mu\text{L}$ and 1 $\text{pg}/\mu\text{L}$ templates concentration after post-PCR procedure (25 cycles) were determined by 6.0 and 6.3% for the E gene and 9.5 and 9.8% for the RdRP gene, respectively.

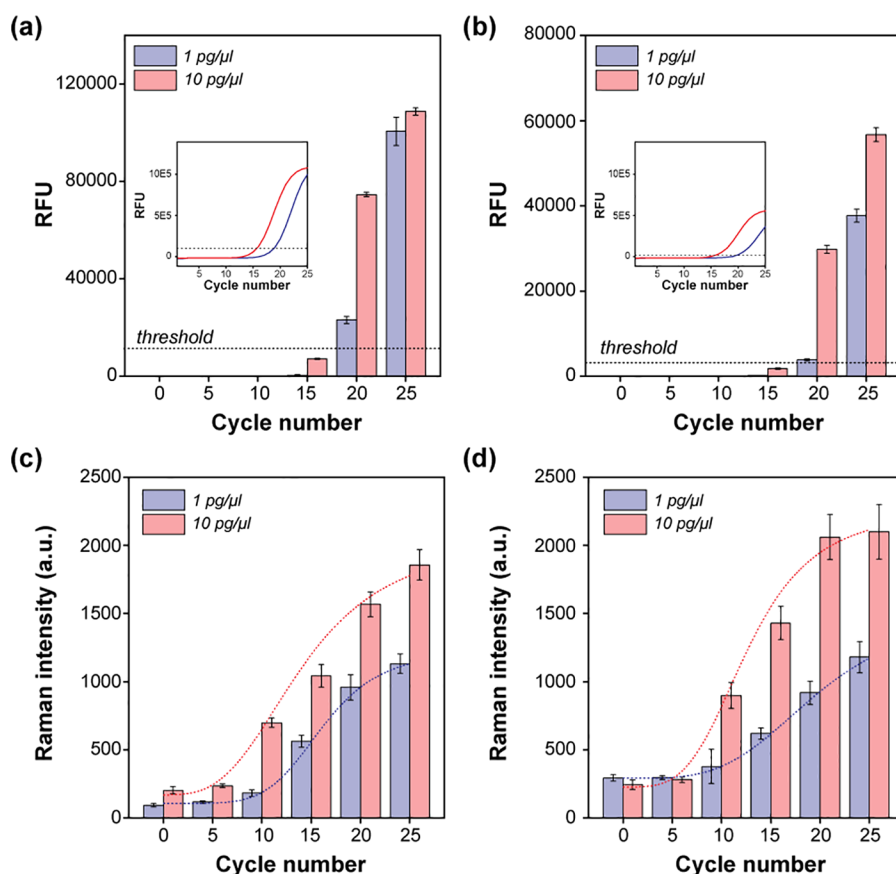


Figure 6. Comparison between (a,b) real-time PCR and (c,d) SERS-PCR. The variation in the fluorescence intensity of two-plex real-time PCR assay with the cycle number is plotted for the (a) E gene and (b) RdRP gene with template concentrations of 1 and 10 pg/μL, respectively. Insets show amplification plots of real-time PCR assay for 1 (blue line) and 10 pg/μL (red line). SERS intensity of two-plex SERS-PCR assay for (c) E gene and (d) RdRP gene with template concentrations of 1 and 10 pg/μL, respectively. The logistic fittings of SERS intensity depending on cycle number for 1 (blue line) and 10 pg/μL (red line) are shown with $R^2 > 0.99$.

In this study, we combined PCR and SERS by adding specific probes in the PCR reaction and subsequently detecting multiple fluorescence dyes targeting different genes via low-cost SERS substrates. In this assay, the 5' fluorophores and 3' biotin-modified probes enabled the separation of fluorescent dyes with streptavidin-coated magnetic beads. The first contribution of this work is to minimize carryover contamination in diagnostic tests, as only fluorescence dyes isolated from PCR products are used for detection. Only the hydrolytically cleaved probe at 5' was used for SERS measurements. The second contribution is the multiplex capability under existing PCR conditions without any modification of primer and probe sequences. Most SERS-PCR assays use complexed primers and programmed detection probes for SERS measurement; however, our method can be universally expanded to other PCR assays. We can easily accomplish multiplex detection through conjugation of individual SERS signaling molecules at the end of the probe sequences. The third contribution is the highly sensitive SERS substrates with quasi-ordered hotspots via a low-cost fabrication method. The complex hierarchical ultrastructures of the cellulose fiber matrixes enable highly sensitive SERS detection, even at low concentrations. In this experiment, the assay detection limit of SERS-PCR was lower than that of real-time PCR. These observations provide insights into the reduction of PCR cycles using highly sensitive SERS. We believe that this technology is innovative and has the potential

to be developed into a powerful tool for rapid, sensitive, and specific diagnosis.

■ ASSOCIATED CONTENT

Supporting Information

The Supporting Information is available free of charge at <https://pubs.acs.org/doi/10.1021/acs.analchem.0c05285>.

PCR and bioplasmonic paper preparation; magnetic bead separation; UV-vis, fluorescence, and SERS measurements; additional figures; and sequence information for oligonucleotides used in this work (PDF)

■ AUTHOR INFORMATION

Corresponding Author

Minhee Kang – Biomedical Engineering Research Center, Smart Healthcare Research Institute, Samsung Medical Center, Seoul 06351, Republic of Korea; Department of Medical Device Management and Research, SAIHST (Samsung Advanced Institute for Health Sciences & Technology), Sungkyunkwan University, Seoul 06355, Republic of Korea; orcid.org/0000-0003-0330-7828; Phone: +82-6007-5436; Email: minhee.kang@samsung.com, minikang@skku.edu

Authors

Eun Ju Kim – Biomedical Engineering Research Center, Smart Healthcare Research Institute, Samsung Medical Center, Seoul 06351, Republic of Korea; Department of Medical Device Management and Research, SAIHST (Samsung Advanced Institute for Health Sciences & Technology), Sungkyunkwan University, Seoul 06355, Republic of Korea

Hanbi Kim – Biomedical Engineering Research Center, Smart Healthcare Research Institute, Samsung Medical Center, Seoul 06351, Republic of Korea; Department of Medical Device Management and Research, SAIHST (Samsung Advanced Institute for Health Sciences & Technology), Sungkyunkwan University, Seoul 06355, Republic of Korea

Eunyoung Park – Biomedical Engineering Research Center, Smart Healthcare Research Institute, Samsung Medical Center, Seoul 06351, Republic of Korea; Department of Medical Device Management and Research, SAIHST (Samsung Advanced Institute for Health Sciences & Technology), Sungkyunkwan University, Seoul 06355, Republic of Korea

Taekyung Kim – Biomedical Engineering Research Center, Smart Healthcare Research Institute, Samsung Medical Center, Seoul 06351, Republic of Korea

Doo Ryeon Chung – Center for Infection Prevention and Control, Samsung Medical Center, Seoul 06351, Republic of Korea; Asia Pacific Foundation for Infectious Diseases (APFID), Seoul 06367, Republic of Korea; Division of Infectious Diseases, Department of Internal Medicine, Samsung Medical Center, Sungkyunkwan University School of Medicine, Seoul 06351, Republic of Korea

Young-Man Choi – Department of Mechanical Engineering, Ajou University, Suwon-si, Gyeonggi-do 16490, Republic of Korea

Complete contact information is available at:

<https://pubs.acs.org/10.1021/acs.analchem.0c05285>

Author Contributions

The manuscript was written through contributions of all authors. All authors have given approval to the final version of the manuscript.

Notes

The authors declare no competing financial interest.

ACKNOWLEDGMENTS

This work was supported by a National Research Foundation of Korea (NRF) grant funded by the Korean government (MSIT) [Grant No. 2019R1A2C2087631, Grant No. 2016M3A9B6919189, and Grant No. 2016M3A9B6919187], by the Korea Medical Device Development Fund grant funded by the Korea government (the Ministry of Science and ICT, the Ministry of Trade, Industry and Energy, the Ministry of Health & Welfare, Republic of Korea, the Ministry of Food and Drug Safety [Grant No. 202011A04], and Samsung Research Funding & Incubation Center of Samsung Electronics [Project Number SRFC-IT1902-05].

REFERENCES

(1) Langer, J.; Jimenez de Aberasturi, D.; Aizpurua, J.; Alvarez-Puebla, R. A.; Auguie, B.; Baumberg, J. J.; Bazan, G. C.; Bell, S. E. J.; Boisen, A.; Brolo, A. G.; Choo, J.; Cialla-May, D.; Deckert, V.; Fabris, L.; Faulds, K.; Garcia de Abajo, F. J.; Goodacre, R.; Graham, D.; Haes, A. J.; Haynes, C. L.; et al. *ACS Nano* **2020**, *14*, 28–117.

(2) Fan, M.; Andrade, G. F. S.; Brolo, A. G. *Anal. Chim. Acta* **2020**, *1097*, 1–29.

(3) Liu, Y.; Zhou, H.; Hu, Z.; Yu, G.; Yang, D.; Zhao, J. *Biosens. Bioelectron.* **2017**, *94*, 131–140.

(4) McNay, G.; Eustace, D.; Smith, W. E.; Faulds, K.; Graham, D. *Appl. Spectrosc.* **2011**, *65*, 825–837.

(5) Chen, H.; Kou, X.; Yang, Z.; Ni, W.; Wang, J. *Langmuir* **2008**, *24*, 5233–5237.

(6) Lei, D. Y.; Li, J.; Fernandez-Dominguez, A. I.; Ong, H. C.; Maier, S. A. *ACS Nano* **2010**, *4*, 432–438.

(7) Kang, M.; Kim, J. J.; Oh, Y. J.; Park, S. G.; Jeong, K. H. *Adv. Mater.* **2014**, *26*, 4510–4514.

(8) Perney, N. M.; Baumberg, J. J.; Zoorob, M. E.; Charlton, M. D.; Mahnkopf, S.; Netti, C. M. *Opt. Express* **2006**, *14*, 847–857.

(9) Hossain, M. K.; Kitahama, Y.; Huang, G. G.; Han, X.; Ozaki, Y. *Anal. Bioanal. Chem.* **2009**, *394*, 1747–1760.

(10) Restaino, S. M.; White, I. M. *Lab Chip* **2018**, *18*, 832–839.

(11) Vo-Dinh, T.; Yan, F.; Wabuyele, M. B. *J. Raman Spectrosc.* **2005**, *36*, 640–647.

(12) Nguyen, A. H.; Lee, J. U.; Sim, S. J. *J. Opt.* **2015**, *17*, 114022.

(13) Wu, Y.; Choi, N.; Chen, H.; Dang, H.; Chen, L.; Choo, J. *Anal. Chem.* **2020**, *92*, 2628–2634.

(14) Kang, T.; Yoo, S. M.; Yoon, I.; Lee, S. Y.; Kim, B. *Nano Lett.* **2010**, *10*, 1189–1193.

(15) Wee, E. J.; Wang, Y.; Tsao, S. C.; Trau, M. *Theranostics* **2016**, *6*, 1506–1513.

(16) Lyu, N.; Rajendran, V. K.; Diefenbach, R. J.; Charles, K.; Clarke, S. J.; Engel, A.; Sydney Colorectal Cancer Study, I.; Rizos, H.; Molloy, M. P.; Wang, Y. *Nanotheranostics* **2020**, *4*, 224–232.

(17) Smith, M.; Smith, K.; Olstein, A.; Oleinikov, A.; Ghindilis, A. *Sensors* **2020**, *20*, 3873.

(18) Yoo, S. M.; Kang, T.; Kim, B.; Lee, S. Y. *Chem. - Eur. J.* **2011**, *17*, 8657–8662.

(19) Li, X.; Yang, T.; Li, C. S.; Song, Y.; Lou, H.; Guan, D.; Jin, L. *Theranostics* **2018**, *8*, 1678–1689.

(20) Hao, Z.; Mansuer, M.; Guo, Y.; Zhu, Z.; Wang, X. *Talanta* **2016**, *146*, 533–539.

(21) Li, M.; Cushing, S. K.; Liang, H.; Suri, S.; Ma, D.; Wu, N. *Anal. Chem.* **2013**, *85*, 2072–2078.

(22) Chen, C.; Liu, W.; Tian, S.; Hong, T. *Sensors* **2019**, *19*, 1712.

(23) Koo, K. M.; Wee, E. J.; Mainwaring, P. N.; Wang, Y.; Trau, M. *Small* **2016**, *12*, 6233–6242.

(24) Ki, J.; Kim, J.; Han, S.; Jang, E.; Lee, T.; Wi, J.-S.; Lee, T. G.; Na, W.; Song, D.; Haam, S. *Opt. Mater. Express* **2017**, *7*, 3136–3136.

(25) Persing, D. H. *J. Clin. Microbiol.* **1991**, *29*, 1281–1285.

(26) Aslanzadeh, J. *Ann. Clin. Lab. Sci.* **2004**, *34*, 389–396.

(27) Ghosh, S. S.; Eis, P. S.; Blumeyer, K.; Fearon, K.; Millar, D. P. *Nucleic Acids Res.* **1994**, *22*, 3155–3159.

(28) Liu, H.; Li, S.; Tian, L.; Liu, L.; He, N. *J. Nanosci. Nanotechnol.* **2010**, *10*, 5311–5315.

(29) Zhou, X.; Xing, D.; Tang, Y.; Chen, W. R. *PLoS One* **2009**, *4*, e8074.

(30) Danielli, A.; Porat, N.; Ehrlich, M.; Arie, A. *Curr. Pharm. Biotechnol.* **2010**, *11*, 128–137.

(31) Wittwer, C. T.; Herrmann, M. G.; Moss, A. A.; Rasmussen, R. P. *BioTechniques* **1997**, *22*, 130–1.

(32) Esbin, M. N.; Whitney, O. N.; Chong, S.; Maurer, A.; Darzacq, X.; Tjian, R. *RNA* **2020**, *26*, 771.

(33) Dorlass, E. G.; Monteiro, C. O.; Viana, A. O.; Soares, C. P.; Machado, R. R. G.; Thomazelli, L. M.; Araujo, D. B.; Leal, F. B.; Candido, E. D.; Telezynski, B. L.; Valerio, C. A.; Chalup, V. N.; Mello, R.; Almeida, F. J.; Aguiar, A. S.; Barrientos, A. C. M.; Suciupira, C.; De Paulis, M.; Safadi, M. A. P.; Silva, D. G. B. P.; Sodre, J. J. M.; Soledade, M. P.; Matos, S. F.; Ferreira, S. R.; Pinez, C. M. N.; Buonafina, C. P.; Pieroni, L. N. F.; Malta, F. M.; Santana, R. A. F.; Souza, E. C.; Fock, R. A.; Pinho, J. R. R.; Ferreira, L. C. S.; Botosso, V. F.; Durigon, E. L.; Oliveira, D. B. L. *Braz. J. Microbiol.* **2020**, *51*, 1117–1123.

(34) Wu, F.; Zhao, S.; Yu, B.; Chen, Y. M.; Wang, W.; Song, Z. G.; Hu, Y.; Tao, Z. W.; Tian, J. H.; Pei, Y. Y.; Yuan, M. L.; Zhang, Y. L.; Dai, F. H.; Liu, Y.; Wang, Q. M.; Zheng, J. J.; Xu, L.; Holmes, E. C.; Zhang, Y. Z. *Nature* **2020**, *579*, 265–269.

(35) Acter, T.; Uddin, N.; Das, J.; Akhter, A.; Choudhury, T. R.; Kim, S. *Sci. Total Environ.* **2020**, *730*, 138996.

(36) Chu, D. K. W.; Pan, Y.; Cheng, S. M. S.; Hui, K. P. Y.; Krishnan, P.; Liu, Y.; Ng, D. Y. M.; Wan, C. K. C.; Yang, P.; Wang, Q.; Peiris, M.; Poon, L. L. M. *Clin. Chem.* **2020**, *66*, 549–555.

(37) Corman, V. M.; Landt, O.; Kaiser, M.; Molenkamp, R.; Meijer, A.; Chu, D. K.; Bleicker, T.; Brunink, S.; Schneider, J.; Schmidt, M. L.; Mulders, D. G.; Haagmans, B. L.; van der Veer, B.; van den Brink, S.; Wijsman, L.; Goderski, G.; Romette, J. L.; Ellis, J.; Zambon, M.; Peiris, M. *Eurosurveill* **2020**, *25*, 2000045.

(38) Holshue, M. L.; DeBolt, C.; Lindquist, S.; Lofy, K. H.; Wiesman, J.; Bruce, H.; Spitters, C.; Ericson, K.; Wilkerson, S.; Tural, A.; Diaz, G.; Cohn, A.; Fox, L.; Patel, A.; Gerber, S. I.; Kim, L.; Tong, S.; Lu, X.; Lindstrom, S.; Pallansch, M. A.; et al. *N. Engl. J. Med.* **2020**, *382*, 929–936.

(39) Ahn, D. G.; Shin, H. J.; Kim, M. H.; Lee, S.; Kim, H. S.; Myoung, J.; Kim, B. T.; Kim, S. J. *J. Microbiol. Biotechnol.* **2020**, *30*, 313–324.

(40) Negri, P.; Flaherty, R. J.; Dada, O. O.; Schultz, Z. D. *Chem. Commun. (Cambridge, U. K.)* **2014**, *50*, 2707–2710.

(41) Jung, H.; Park, M.; Kang, M.; Jeong, K. H. *Light: Sci. Appl.* **2016**, *5*, e16009.

(42) Kang, M.; Park, S. G.; Jeong, K. H. *Sci. Rep.* **2015**, *5*, 14790.

(43) Kang, M.; Ahn, M.-S.; Lee, Y.; Jeong, K.-H. *ACS Appl. Mater. Interfaces* **2017**, *9*, 37154–37159.

(44) Liu, Y.; Zhang, Y.; Tardivel, M.; Lequeux, M.; Chen, X.; Liu, W.; Huang, J.; Tian, H.; Liu, Q.; Huang, G.; Gillibert, R.; de la Chapelle, M. L.; Fu, W. *Plasmonics* **2020**, *15*, 743–752.

(45) Thomsen, V.; Schatzlein, D.; Mercurio, D. *Spectroscopy* **2003**, *18*, 112–114.

(46) Dougan, J. A.; Faulds, K. *Analyst* **2012**, *137*, 545–554.